Numerical and Experimental Study of Strain Rate Effects in Laser Forming

Wenchuan Li

Y. Lawrence Yao[1]

Department of Mechanical Engineering,
Columbia University,
New York, NY 10027

Experimental investigation and numerical simulation of the influence of the strain rate in laser forming are presented. To isolate and effectively study the strain rate effects, which are temperature dependent, a ''constant peak temperature'' method is developed with the aid of numerical modeling and solution. Under the condition of the constant peak temperature, the effects of strain rate on forming efficiency, residual stress and hardness of the formed parts are studied both experimentally and numerically. In the numerical model, the temperature dependence and strain-rate dependence of the flow stress and other material properties are considered. The simulation results are consistent with the experimental observations. [S1087-1357(00)01004-2]

1 Introduction

Laser forming is a process in which laser-induced thermal distortion is used to form sheet metal without a hard forming tool or external forces. It is therefore a flexible forming technique suitable for low-volume production and/or rapid prototyping of sheet metal, as well as for adjusting and aligning sheet metal components [1]. Aerospace, shipbuilding, microelectronics and automotive industries have shown interest. A simple type of the laser forming is straight-line laser bending (Fig. 1) and more involved shapes can also be generated by the process.

Understanding various aspects of laser forming is a challenging problem of considerable theoretical and practical interest. Experimental and theoretical investigations have been reported to understand the mechanisms involved in laser forming. The proposed mechanisms are the temperature gradient mechanism (TGM) [2], buckling mechanism (BM) [3], and upsetting mechanism depending on operation conditions, material properties and workpiece geometry. A number of analytical models were derived to predict the bending angle α_b (Fig. 1) in the straight-line laser bending [2]. Some of the models are in reasonable agreement with experimental results. More detailed studies were conducted via numerical investigations. Vollertsen et al. [4], Hsiao et al. [5], and Alberti et al. [6] simulated the process using the finite element or finite difference method. In these numerical studies, the bending angle was computed and compared reasonably with experimental results. Additional information, such as temperature, stress and strain distribution and time history, were also extracted for more detailed analysis. Parametric studies of process parameters, workpiece geometry and material properties on the laser forming process were reported, such as influence of strain hardening [7], and edge effects [8,9]. Issues of working accuracy [10], and aerospace alloy application [11] have also been reported.

The effects of strain rate in the laser forming, however, have not been studied in detail. In the laser forming, the strain rate could reach two per second under commonly used laser power levels and laser scanning velocities. Although this level of strain rate is not high as compared with that experienced in some other metal forming processes, temperature in the laser forming could rise close to the melting point of the workpiece material. As known, the strain rate at elevated temperatures has much higher influence on the material flow stress than at lower temperatures. The influence on the flow stress translates to that on the forming process and properties of the formed parts, including residual stresses and hardness of the formed parts.

Experimental results showed that the bend angle α_b in the straight-line laser bending is directly proportional to $v^{-0.63}$ for low-carbon steel plates [2] or $v^{-0.54}$ for aluminum metals [11] where v is the laser scanning velocity (therefore associated with the strain rate). The main reason that the bend angle decreases with increasing velocity is that the laser energy input per unit time reduces when the scanning velocity increases. The bend angle decrease is also due to flow stress increase because the higher the velocity, the higher the strain rate, which causes the flow stress to rise. Therefore, aforementioned relationships represent the effects of both the input energy and the strain rate on the bending process. One may lead to think that a better approach to explore the strain rate effects is to ensure a constant laser energy input per unit length, that is, to keep the line energy, P/v, constant, where P is the laser power. If the units of P and v are W and m/s, the unit of the line energy is J/m. Under the condition of constant line energy, although the laser energy input per unit length is kept constant, the net energy input available for the forming purpose may still vary due to different time available for heat dissipation associated with different scanning velocities. Therefore, the ideal scenario is to ensure the *net* energy input available for the forming purpose constant while the strain rate is varied. In this way the strain rate effects can be isolated and studied without interference of other variables.

In this work, strain rate effects in laser bending are studied under the condition of ''constant peak temperature,'' that is, the combinations of laser power and scanning velocity are so determined that the peak temperature reached at the top surface of the laser scanned workpiece remains constant. In this way the net energy input available for the forming purpose can be kept approximately constant under different scanning velocity (strain

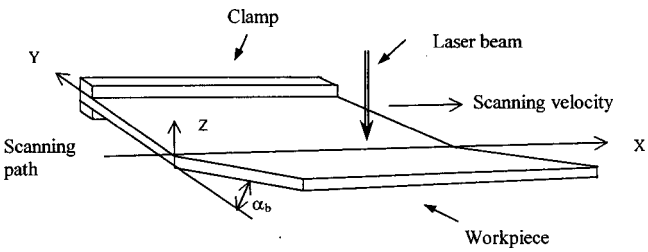

Fig. 1 Schematic of straight-line laser bending

[1]Corresponding author.

Contributed by the Manufacturing Engineering Division for publication in the JOURNAL OF MANUFACTURING SCIENCE AND ENGINEERING. Manuscript received July 1999; revised Jan. 2000. Associate Technical Editor: K. Stelson.

rate). A numerical model based on the finite element method is developed to aid the determination of the process parameter values that give the constant peak temperature. The same model is also used to predict the effects of strain rate on bending angle and residual stress among others. The numerical results are experimentally validated.

2 Strain Rate and Effects

For a given temperature, the strain rate in terms of tensor $\dot{\underline{\underline{\varepsilon}}}$ can be written as

$$\dot{\underline{\underline{\varepsilon}}} = \frac{1}{2}\left(\frac{\partial \underline{v}}{\partial \underline{x}} + \left(\frac{\partial \underline{v}}{\partial \underline{x}}\right)^T\right) \tag{1}$$

where $\underline{v}$ is the particle velocity vector and is defined as $\underline{v} = \partial \underline{x}/\partial t$ when the Lagrangian viewpoint is taken, $\underline{x}$ is the spatial position vector of a material particle at time t, and $\partial \underline{v}/\partial \underline{x}$ is the velocity gradient, all in the current configuration. The strain rate can be decomposed as

$$\dot{\underline{\underline{\varepsilon}}} = \dot{\underline{\underline{\varepsilon}}}^{el} + \dot{\underline{\underline{\varepsilon}}}^{pl} \tag{2}$$

where $\dot{\underline{\underline{\varepsilon}}}^{el}$ and $\dot{\underline{\underline{\varepsilon}}}^{pl}$ are the elastic and inelastic strain rate, provided that the principal values of the elastic strain $\underline{\underline{\varepsilon}}^{el}$ are much smaller than unity, which is true for most metallic materials. When the thermal strain rate $\dot{\underline{\underline{\varepsilon}}}^{th}$ has to be considered, the additive strain rate decomposition can be extended as

$$\dot{\underline{\underline{\varepsilon}}} = \dot{\underline{\underline{\varepsilon}}}^{el} + \dot{\underline{\underline{\varepsilon}}}^{pl} + \dot{\underline{\underline{\varepsilon}}}^{th} \tag{3}$$

provided that the elastic and thermal strains are relatively small. The strain due to creep is not considered here because of the nature of the laser forming process.

The relation between strain ε_{ij} and stress σ_{ij} under plastic deformation can be written as

$$d\varepsilon_{ij} = (d\lambda)\frac{\partial f}{\partial \sigma_{ij}} \tag{4}$$

where $d\lambda$ is the proportionality factor (plastic compliance), f is the yield function and temperature is not considered. When Von Mises criterion is applied for f, Eq. (4) takes the following form.

$$d\varepsilon_1 : d\varepsilon_2 : d\varepsilon_3 = [\sigma_1 - \tfrac{1}{2}(\sigma_2+\sigma_3)] : [\sigma_2 - \tfrac{1}{2}(\sigma_3+\sigma_1)] : [\sigma_3 - \tfrac{1}{2}(\sigma_1+\sigma_2)] \tag{5}$$

where σ_1, σ_2, and σ_3 are the principal stresses.

The stress and strain tensor, σ_{ij} and ε_{ij}, can be decomposed into their mean portions and their deviatoric portions, that is, $\sigma = \sigma_{ii}/3$, $\varepsilon = \varepsilon_{ii}/3$, $s_{ij} = \sigma_{ij} - \delta_{ij}\sigma$, and $e_{ij} = \varepsilon_{ij} - \delta_{ij}\varepsilon$, where σ and ε are mean portion, s_{ij} and e_{ij} are deviatoric portions, and δ_{ij} is the Kronecker delta. For work-hardening materials, the relationship between deviatoric stress and plastic strain rate $\dot{e}_{ij}{}^{pl}$ by taking into consideration of temperature influence can be written in terms of tensor [12].

$$\dot{e}_{ij}{}^{pl} = 0, \quad \text{if } f<0, \text{ or if } f=0 \quad \text{and} \quad \left(\frac{\partial f}{\partial s_{ij}}\dot{s}_{ij} + \frac{\partial f}{\partial T}\dot{T}\right) < 0$$

$$\dot{e}_{ij}{}^{pl} = -\frac{1}{\dfrac{\partial f}{\partial e_{ij}{}^{pl}}}\left(\frac{\partial f}{\partial s_{kl}}\dot{s}_{kl} + \frac{\partial f}{\partial T}\dot{T}\right), \tag{6}$$

$$\text{if } f=0 \quad \text{and} \quad \left(\frac{\partial f}{\partial s_{ij}}\dot{s}_{ij} + \frac{\partial f}{\partial T}\dot{T}\right) \geqslant 0$$

Equation (6) represents the general relation of stress, strain and their rates, in terms of tensor and with temperature consideration. In practice, however, similar relationships are often empirically determined under the one-dimensional condition and applied to multidimensional cases using the concept of equivalent stress and strain. Much effort therefore has been made to determine the flow stress dependence on strain rate and temperature for the one-dimensional case.

For a deformation process of metals with a stress, σ, and temperature, T, the strain rate, $\dot{\varepsilon}$, is given by [13]

$$\dot{\varepsilon} = K\left(\sinh\left(\frac{V\sigma}{RT}\right)\right)^{1/m} e^{-Q/RT} \tag{7}$$

where K is a constant, V a constant with dimensions of volume, R the gas constant, m the strain-rate sensitivity exponent, and Q the activation energy. If $\sigma \ll RT/V$, Eq. (7) can be rewritten as

$$\sigma = C'\dot{\varepsilon}^m e^{mQ/RT} = C\dot{\varepsilon}^m \tag{8}$$

where both coefficient C and strain-rate sensitivity exponent m depend on temperature and material.

3 Numerical Simulation

To simulate the strain rate effects in laser forming, reasonable values of the strain-rate sensitivity exponent m, which is temperature-dependent, are necessary. The following equation can be obtained from Eq. (8)

$$m = \ln\frac{\sigma_2}{\sigma_1}\Big/\ln\frac{\dot{\varepsilon}_2}{\dot{\varepsilon}_1} \tag{9}$$

and m can therefore be experimentally determined. Many empirical expressions for the sensitivity exponent m have been proposed for different materials and temperature ranges. An example for low carbon steels at relatively higher temperatures is [14]

$$m = \frac{(T-873)}{4{,}330 - 895\sinh(C)} + 0.034 \tag{10}$$

where T is absolute temperature and C carbon content in terms of weight percentage.

In this work, however, strain-rate and temperature dependent flow stress is directly determined because the numerical solver used requires the flow stress instead of m as an input. Since low carbon steels are of interest in this work, the following empirical relations of the flow stress, σ, are adopted [15,16]. These relationships were obtained through uniaxial tension and/or compression tests at certain temperatures.

For $293\,\text{K} < T < 573\,\text{K}$

$$\sigma = \sigma_s + (8.2 + 1.3\varepsilon \cdot e^{-0.0135\varepsilon}) \cdot (0.97e^{0.0007\dot{\varepsilon}}) \cdot (1.14 - 0.0023T) \tag{11}$$

where σ_s is the static yield stress at 293 K.

For $T > 293\,\text{K}$

$$\sigma = A(T)\left(\frac{\dot{\varepsilon}}{1000}\right)^{0.0195}\varepsilon^{0.21} \tag{12}$$

where $A(T)$ is

$$A(T) = 1394e^{-0.00118\cdot T} + 339\exp\left(-0.0000184\left(T - \left(943 + 23.5\ln\frac{\dot{\varepsilon}}{1000}\right)\right)^2\right) \tag{13}$$

The main assumptions used in the numeral simulation of laser forming are as follows. The materials simulated in this work are isotropic and continuous. Plastic deformation generated heat is small as compared to energy input in the laser forming so that it is negligible. During the entire laser forming process, no melting takes place. The forming process is symmetrical about the laser-scanning path (Fig. 1).

The boundary conditions used include the top surface being cooled by a weak gas flow. The remaining surfaces are cooled through free convection with atmosphere. Across the symmetric plane (the X-Z plane in Fig. 1), the movement of materials in the

Y direction does not occur. The symmetric surface is under the adiabatic condition. Surface heat flux follows $q=q(\underline{x},t)$, surface convection $q=h(T-T^0)$, where $h=h(\underline{x},t)$ is the film coefficient, and $T^0=T^0(\underline{x},t)$ the surrounding temperature, and radiation $q=A((T-T^z)^4-(T^0-T^z)^4)$, where A is the radiation constant and T^z the absolute zero on the temperature scale used.

The finite element numerical analysis was made using code ABAQUS version 5.7-1. The simulation of the laser forming process was realized by a thermal-structure analysis. For thermal and structural analysis, the same mesh model is used. In order to simulate the shear process in the laser forming, a three-dimension element with twenty nodes was used because this kind of element has no shear locking and hourglass stiffness and is also compatible with thermal stress analysis. A user-defined FORTRAN program was necessary to model the heat source input from the Gaussian laser beam.

4 Experiment

As discussed early, in order to study the strain rate effects in an isolated manner, it is desirable to create conditions under which strain rate may vary but net energy input available for the forming purpose remains constant. To approximate the scenario, a constant peak temperature method was devised. In determining the process parameters for the condition of constant peak temperature, seven values of the scanning velocities were specified first (Table 1). A targeted peak temperature at the top surface of the workpiece, 1,030°C, was also specified. For each velocity, the corresponding laser power was iteratively determined using the numerical simulation. The criterion used in the determination was whether a power level in combination with a specified velocity will approximately yield the targeted peak temperature. If not, the iteration is continued. The seven power levels determined using this procedure are listed in Table 1. The predicted peak temperature under five of them is shown in Fig. 4.

Please note that for a specific combination of velocity and power, the peak temperature remains approximately constant throughout the scanning path except at both ends of the path [9]. This fact makes the constant peak temperature method possible where the peak temperature refers to the peak temperature throughout the path and ignores the temperature change at both ends of the path.

For comparison purpose, key experimental results under the condition of constant line energy [17] are also included in Section 5 below. The conditions listed in Table 2 are for 10 J/mm.

Laser bending experiments were carried out with a PRC1500 CO_2 laser system with the maximum power of 1.5 kW. The distribution of the power density is Gaussian (TEM_{00}). The diameter of the laser beam used is 4 mm, which is defined as the diameter at which the power density becomes $1/e^2$ of the maximum power value. The samples were made of low carbon steel AISI 1010 and 80 mm by 40 mm by 0.89 mm in size, with 40 mm along the scanning direction. The samples were first cleaned using propanol and then coated with graphite following the procedure reported by Arnet and Vollertson [3]. The absorption coefficient of 0.6 reported by them was used in the numerical simulation of this work. The temperature dependency of the absorption characteristics was not considered. The geometry of the samples was measured before and after laser forming using a coordinate measuring machine. During the laser scanning, the samples were clamped at one side (Fig. 1). The bend angle may vary slightly along the scanning direction and an average angle was calculated for each sample after measuring at a few locations along the scanning direction. The residual stress was measured using X-ray diffractometry.

Table 1 Experimental and simulation condition under constant peak temperature

Velocity (mm/s)	80	90	100	110	120	140	170
Power (W)	800	843	886	929	970	1040	1130

Table 2 Experimental and simulation condition under constant line energy

Velocity (mm/s)	40	60	80	100	120	135	138
Power (W)	400	600	800	1000	1200	1350	1380

5 Results and Discussion

The results under the condition of constant line energy are briefly presented first (Figs. 2 and 3) as a comparison. These results except the simulation results of bending angle without consideration of the strain rate effects (the dotted line in Fig. 2) are from Li and Yao [17]. The rest of results are obtained under the condition of constant peak temperature. All results of temperature, strain and stress are for the scanning path of a workpiece, at the top surface, middle plane, bottom surface or throughout the thickness direction as noted in the figures.

5.1 Constant Line Energy. Figure 2 shows the variation of bend angle with scanning speed under the constant line energy of 10 J/mm (Table 2). It is seen that at lower velocities, the bend angle is smaller despite the line energy being held constant. This

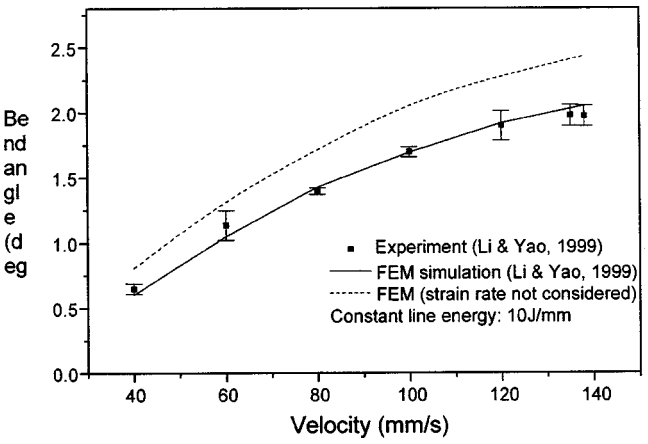

Fig. 2 Experimental and numerical bend angle under constant line energy

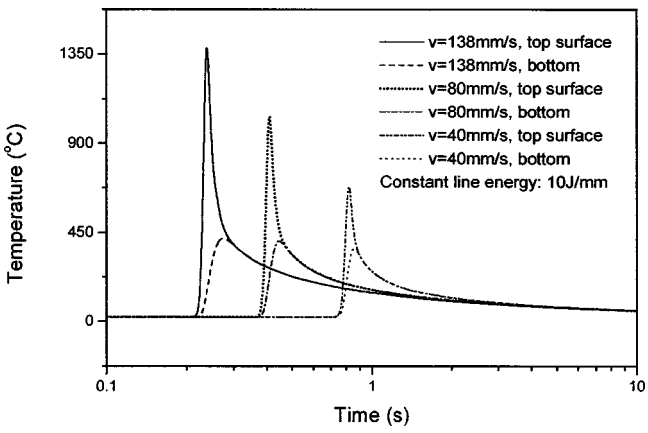

Fig. 3 Simulated time histories of temperature under the condition of constant line energy [17]

is because when the scanning velocity is lower the through-thickness temperature gradient is smaller. This in turn makes the difference between the thermally induced distortions at the top and bottom surfaces smaller. More importantly, heat dissipation is more significant at lower speeds and that makes the efficiency of the forming process to decrease. The numerical results closely agree with the experimental data.

Shown in Fig. 2 in a dotted line is the predicated bend angle without considering the strain rate effects on the flow stress (the temperature dependency of the flow stress still considered). It can be seen that the predicted bending angle is larger without considering the strain rate effects obviously because the increase in the flow stress due to strain rate was left out and therefore larger deformations were predicted. It is also interesting to note that, in relative terms, the bending angle discrepancy at high velocities with and without strain rate consideration is smaller than that at lower velocities. This is because, when the velocity increased, both temperature (Fig. 3) and strain rate increased. The former caused the flow stress to decrease and the latter caused the flow stress to increase. At high velocities, the effect of the former was more dominant and as a result the bending angle discrepancy with and without strain rate consideration is relatively smaller.

Shown in Fig. 3 are simulated time histories of temperature on the top surface of the workpiece along the scanning path. As seen, the peak temperature increases with the velocity even when the line energy is kept constant. This is obviously due to less heat dissipation at the higher velocities. In addition, the temperature difference between the top and bottom surfaces increases with velocity for the same reason.

Figures 2 and 3 show that, at higher velocities, the strain rate increases and so does the temperature. The increase of strain rate causes increase of flow stress but the increase of temperature causes flow stress to fall. It is therefore difficult to pinpoint the effects of the strain rate. The rest of results are obtained under the condition of constant peak temperature.

5.2 Constant Peak Temperature. As seen from Fig. 4, for the specified velocities, the laser power levels were determined via the simulation to give approximately the same peak temperature of 1,030°C at the top surface of workpiece (Table 1). Although the same peak temperature at the top surface does not necessarily mean the same temperature distribution and thermal process, the method of constant temperature ensures that the effect of temperature on flow stress is relatively small and allows one to focus on studying the effects of strain rate (scanning velocity).

It is worth pointing out that under the condition of constant peak temperature, the laser power still increases with the scanning velocity but does not increase as fast as under the condition of constant line energy. The line energy therefore decreases with increase of the scanning velocity (Fig. 5). This is quite understandable because the more significant heat dissipation at lower velocities requires higher line energy to reach the same peak temperature.

Figure 6 compares the simulation and experimental results of the bend angle vs. velocity. In Fig. 7, a comparison of numerical simulation and experimental results is made for the *Y*-axis residual

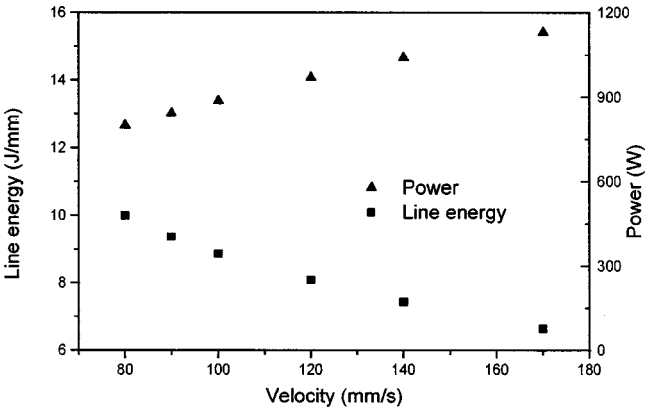

Fig. 5 Experimental values of line energy and laser power under the condition of constant peak temperature

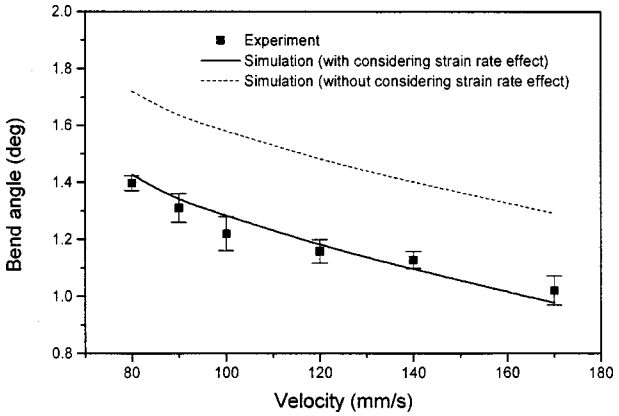

Fig. 6 FEM and experimental bend angle under the condition of constant peak temperature

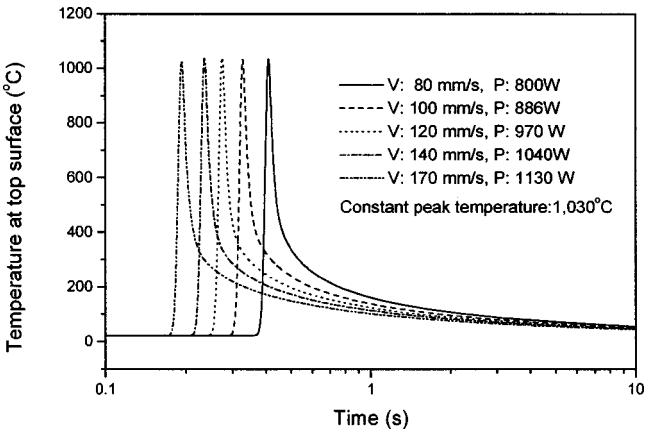

Fig. 4 Simulated time histories of temperature at the top surface under the condition of constant peak temperature

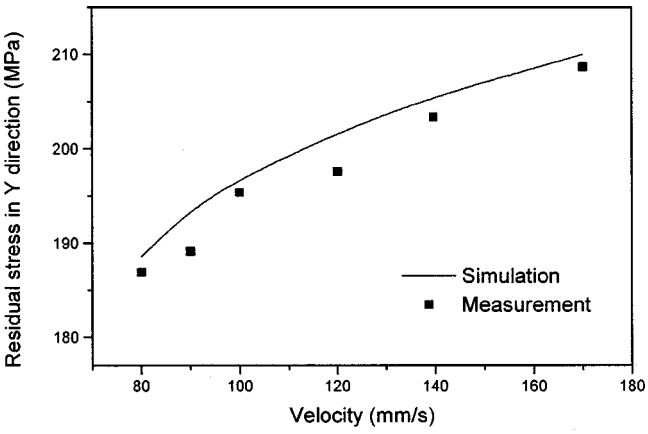

Fig. 7 FEM and X-ray diffraction measurement of residual stress for the samples scanned under the condition of constant peak temperature

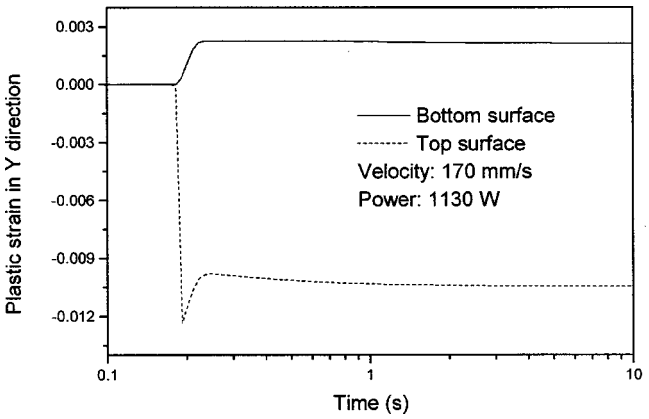

Fig. 8 Typical simulated time histories of plastic strains in the *Y* direction

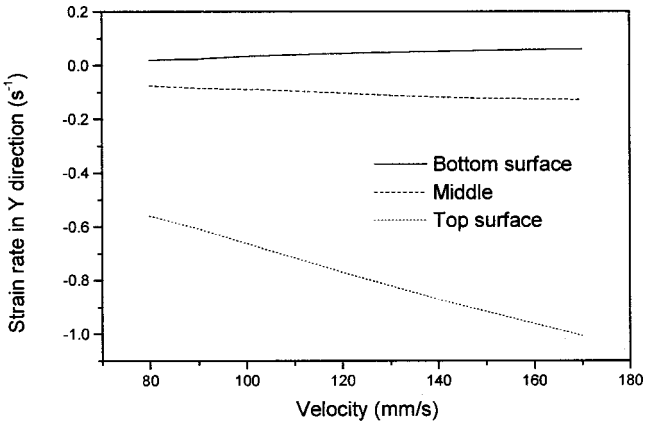

Fig. 10 Simulated strain rate in *Y* direction under the condition of constant peak temperature

stress on the top surface of the workpiece. The yield stress of the material used at room temperature is about 265 MPa. In both figures, the simulation results agree with experimental measurements. The trends, namely, the bend angle decreasing and residual stress increasing with the increase of scanning velocity (strain rate) are consistent with the understanding of the forming mechanisms. They will be further explained, along with results of strain rate and stress time history.

Shown in Fig. 6 in a dotted line is the predicted bending angle without considering the strain rate effects. Similar to Fig. 2, the predicted bending angle is larger without considering the strain rate effects obviously because the increase in the flow stress due to strain rate was left out and therefore larger deformations were predicted. Different from Fig. 2 is that, in relative terms, the bending angle discrepancy at high velocities with and without strain rate consideration is larger than that at lower velocities. This is because the temperature remained about the same over the entire velocity range under this constant peak temperature condition, and therefore the discrepancy was due to the strain rate effects alone. As a result, discrepancy with and without the strain rate consideration is relatively larger at larger strain rates (at higher velocities).

Figure 8 presents a typical simulation result of the time history of plastic strains in the *Y* direction. As seen, the plastic strain is compressive on the upper surface and tensile on the lower surface, which is quite typical for laser forming under the temperature gradient mechanism (TGM). A steep thermal gradient through the thickness leads to a much higher tendency of thermal expansion at the top surface. But the surrounding workpiece material restricts the expansion, resulting significant plastic deformation near the top surface. At the cooling stage, the material that has been compressed in the upper layers contracts so that a shortening of these layers make the workpiece bend towards the laser beam, while the lower layers undergo a slight tension (sometimes a slight compression resulted from the heating stage remains).

Figure 9(*a*) shows a typical simulation contour plot of plastic strain at the symmetric plane. Due to space limitation, only a portion of the plane (0.89 mm thick and 40 mm long), was shown. Figure 9(*b*) shows that, as the scanning velocity increases, the compressive plastic deformation at top surface becomes smaller. This is obviously due to the increase in strain rate associated with the increased velocity (Fig. 10). The increased strain rate in turn causes the increase in flow stress, which makes bending more difficult at the increased velocity. Note that under the constant peak temperature condition, the results in Fig. 9(*b*) primarily represent the effect of strain rate on flow stress because the effect of temperature on flow stress can be neglected. Comparing Figs. 6 and 10, it can be seen that the bend angle decreases about 30 percent for the nearly doubled strain rate. As seen from Fig. 9(*b*), the maximum plastic strain is about 0.016, while the corresponding elastic strain (not shown) is about an order of magnitude smaller than the plastic strain.

(a) Portion (8 mm long) of the symmetric plane (0.89 mm thick and 40 mm long) (Power=843W, Velocity=90mm/s)

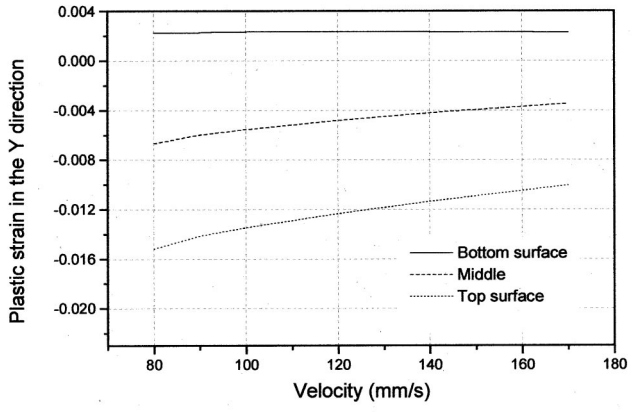

(b)

Fig. 9 Simulated plastic strain in *Y* direction under the condition of constant peak temperature

5.3 Residual Stress. To understand the increase in the *Y*-axis residual stresses with velocity (Fig. 7), the time history of temperature, *Y*-axis plastic strain, and *Y*-axis stress for low and high strain rate cases ($V=80$ mm/s, $P=800$ W, and $V=170$ mm/s, $P=1130$ W) are plotted in Fig. 11. Note that all quantities in Figs. 7 and 11 are for the top surface on the scanning path where more changes take place during forming than at the bottom surface. As seen in Fig. 11, the temperature profiles are expectedly very similar between the two cases because these cases are determined to have the same peak temperature in the first place. But the strain rate and in turn the flow stress are quite different between the two cases.

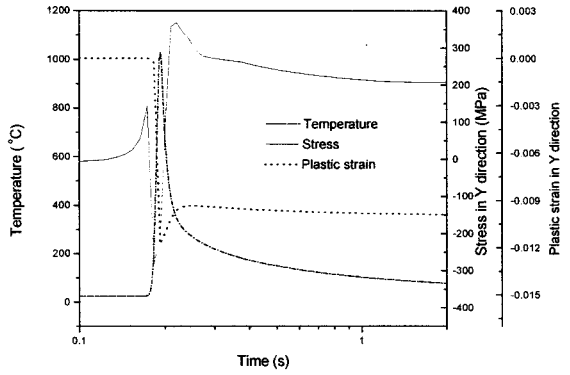

(a) V=170mm/s, P=1130W

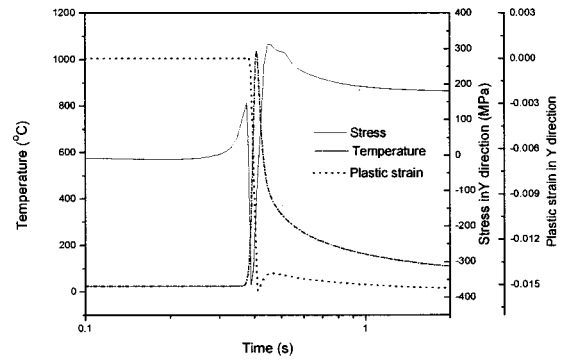

(b) V=80mm/s, P=800W

Fig. 11 Simulated results for comparison of the effect of high and low strain rate on residual stress

It can be seen from the time history of stress that, with the imminent arrival of the laser beam, a small tensile stress first develops due to the expansion of the preceding area, which is being heated by the laser. With the laser beam arrival and temperature rise, material tends to expand but undergoes significant compressive stress due to mechanical constraints of the surrounding material. When temperature rises further, the flow stress decreases and plastic deformation accrues, which releases the compressive stress and the absolute value of the compressive stress starts to reduce. After the temperature reaches its maximum value, the material contracts due to the reduced temperature and the stress starts to change towards being tensile. At the same time, the tensile stress continues to rise as the material immediately ahead is being heated up by the laser beam and expands. Since the flow stress associated with the high velocity (strain rate) is higher, the tensile stress due to the thermal expansion of the material immediately ahead also rises higher. As a result, the residual stress corresponding to the high velocity remains higher than that for the low velocity, although in both cases the stress falls slightly because of the contraction of the material immediately ahead. The effect of strain rate on residual stress, however, is relatively moderate. As seen from Figs. 7 and 10, when the strain rate is nearly doubled between the lower and higher speed cases, the residual stress increases by about 15 percent.

5.4 Hardness. The hardness of the deformed workpiece is measured at the top surface along the scanning path (Fig. 12). The measurement is taken 6 days after the forming is done. As seen, the hardness decreases with the increase of velocity (shown in brackets), because of the effect of work hardening. At lower velocities, the strain rate and thus flow stress is lower, resulting in higher plastic strain. The higher plastic strain leads to more significant work hardening. A simple calculated relationship between

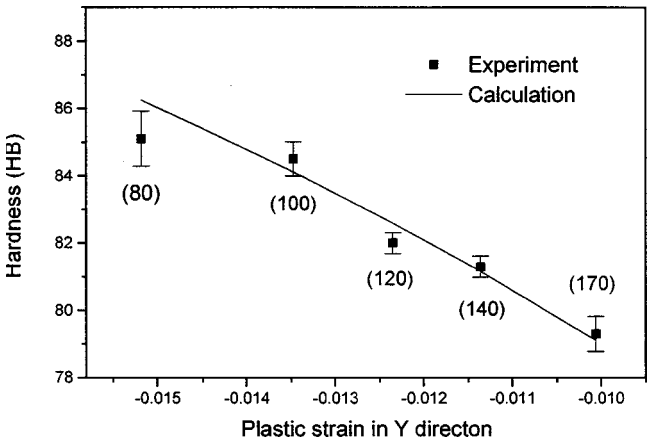

Fig. 12 Hardness vs. simulated plastic strain in *Y* direction under the condition of constant peak temperature (data in brackets are the corresponding scanning velocities in mm/s)

the hardness and plastic strain is also superposed on Fig. 12 that agrees with the measurement data. The calculation is based on the well known empirical relationship between stress and hardness as well as $\sigma = K'\varepsilon^n$, where ε is the simulated plastic strain, n the work-hardening exponent for low carbon steel, and K' constant.

6 Conclusions

Laser forming simulation and experiments are conducted under the condition of constant peak temperature, which largely isolates the effects of strain rate from that of temperature. Strain rate in the laser forming process may not be very high (about 1 /sec. in this work) but the temperature involved is high (up to 1,030°C in this work). This makes the strain rate effects on flow stress and thus deformation in the laser forming process quite significant. The bend angle decreased by about 30 percent for nearly doubled strain rate under the conditions used. Simulation results with and without consideration of the strain rate effects are compared and the difference is indicative of the necessity of considering the strain rate effects. Residual stress in the *Y* direction increased moderately with strain rate. For the nearly doubled strain rate, residual stress increases by about 15 percent under the conditions used. With the same strain rate increase, the hardness at the irradiated surface of the formed samples decreased by about 7 percent due to the reduced work hardening.

Acknowledgments

The authors gratefully acknowledge Mr. J. Bao for his assistance in numerical simulation, and Mr. Jack Tsai and Ms. Dee Breger for their assistance in X-ray diffraction measurement.

References

[1] Magee, J., Watkins, K. G., and Steen, W. M., 1998, ''Advances in laser forming,'' J. Laser Appl., **10**, pp. 235–246.
[2] Vollertsen, F., 1994, ''Mechanism and models for laser forming,'' Laser Assisted Net Shape Engineering, *Proceedings of the LANE'94*, Vol. 1, pp. 345–360.
[3] Arnet, H., and Vollertsen, F., 1995, ''Extending laser bending for the generation of convex shapes,'' IMechE Part B: J. Eng. Manufact., **209**, pp. 433–442.
[4] Vollertsen, F., Geiger, M., and Li, W. M., 1993, ''FDM and FEM simulation of laser forming a comparative study,'' Adv. Technol. Plasticity, **3**, pp. 1793–1798.
[5] Hsiao, Y.-C., Shimizu, H., Firth, L., Maher, W., and Masubuchi, K., 1997, ''Finite element modeling of laser forming,'' *Proc. ICALEO '97*, Section A, pp. 31–40.
[6] Alberti, N., Fratini, L., and Micari, F., 1994, ''Numerical simulation of the laser bending process by a coupled thermal mechanical analysis,'' Laser Assisted Net Shape Engineering, *Proceedings of the LANE'94*, Vol. 1, pp. 327–336.

[7] Sprenger, A., Vollertsen, F., Steen, W. M., and Watkins, K., 1994, ''Influence of strain hardening on laser bending,'' Laser Assisted Net Shape Engineering, *Proceedings of the LANE'94*, Vol. 1, pp. 361–370.
[8] Magee, J., Watkins, K. G., and Steen, W. M., 1997, ''Edge effects in laser forming,'' *Laser Assisted Net Shape Engineering 2, Proceedings of the LANE'97*, Meisenbach Bamberg, pp. 399–406.
[9] Bao, J., and Yao, Y. L., 1999, ''Analysis and predication of edge effects in laser bending,'' *Proc. 18th Int. Congress on Applications of Lasers and Electro-Optics* (ICALEO '99): Conf. on Laser Materials Processing, San Diego, CA.
[10] Hennige, T., Holzer, S., Vollertsen, F., and Geiger, M., 1997, ''On the working accuracy of laser bending,'' J. Mater. Process. Technol., **71**, pp. 422–432.
[11] Magee, J., Watkins, K. G., and Steen, W. M., 1997, ''Laser forming of aerospace alloys,'' *ICALEO '97*, Section E, pp. 156–165.
[12] Boley, B. A., and Weiner, J. H., 1997, *Theory of Thermal Stresses*, Dover, New York.
[13] Hosford, W. F., and Caddell, R. M., 1993, *Metal Forming Mechanics and Metallurgy*, PTR, Prentice-Hall, Englewood Cliffs, NJ.
[14] Schindler, I., Strakos, M., and Sramek, L., 1989, ''Influence of carbon and temperature on the stain rate sensitivity of carbon steel,'' Scr. Metall., **23**, pp. 1669–1672.
[15] Vashchenko, A. P., Suntsov, G. N., Belalova, G. V., and Medvedev, A. A., 1991, ''Mechanical properties of low carbon steels over a wide range of temperature and strain rates applied to processes of thin sheet rolling,'' Strength Mater., **22**, pp. 1205–1214.
[16] Maekawa, K., Shirakashi, T., and Usui, E., 1983, ''Flow stress of low carbon steel at high temperature and strain rate (part 2)—Flow stress under variable temperature and variable strain rate,'' Bull. Jpn. Soc. Precis. Eng., **17**, pp. 167–172.
[17] Li, W., and Yao, Y. L., 1999, ''Laser forming with constant line energy,'' Int. J. Adv. Manufact. Technol., Springer-Verlag, submitted.